HIGH-TEMPERATURE SUPERCONDUCTOR MATERIALS FOR CONTACT LAYERS IN SOLID OXIDE FUEL CELLS: I. SINTERING BEHAVIOR AND PHYSICAL PROPERTIES AT OPERATING TEMPERATURES

F. TIETZ[1]†**, I. ARUL RAJ**[2]**, W. JUNGEN**[1] **and D. STÖVER**[1]

[1]Forschungszentrum Jülich, IWV-1, 52425 Jülich, Germany and [2]Central Electrochemical Research Institute, Karaikudi 630 006, Tamil Nadu, India

Abstract—The superconducting materials $Bi_2Sr_2CaCu_2O_{8+x}$, and $Bi_2Sr_2CuO_{6+x}$ were identified as possible candidates for contact layer materials between the perovskite-type ceramic cathode and the metallic interconnector for intermediate-temperature solid oxide fuel cells (IT-SOFCs). The two compounds were synthesized by solid-state reaction and citrate complexation techniques. Densification experiments were performed in air at different temperatures. It was found that the pressed pellets fabricated from both the phases had undergone shape changes due to swelling at temperatures above 800°C. Since the processes of volume expansion and crystallization were found to compete with the sintering process, it was expected to be very difficult to achieve compact layers from these materials. The conductivity measurements indicated metallic behavior of both phases and rather low conductivity values for application as a contact layer in IT-SOFC. Dilatometric experiments were also carried out on these materials to measure their thermal expansion coefficients. The properties of commercial-grade $YBa_2Cu_3O_{7-x}$ were also investigated for comparison. © 2001 Acta Materialia Inc. Published by Elsevier Science Ltd. All rights reserved.

1. INTRODUCTION

Solid oxide fuel cell (SOFC) development represents one of the central topics in today's energy and environment scenario [1–7]. Owing to the high operating temperature of SOFCs (900–1000°C), several complex and difficult problems still remain to be solved. Among the several cell designs considered (e.g. see Ref. [6]), the planar design offers scope for fabrication and use of cell components with a large apparent geometric area permitting the realization of a large reaction surface area for electron transfer at the electrode–electrolyte interface [8]. In the planar cell design, the unit cell components, that is, nickel–cermet anode, oxide-ion-conducting solid electrolyte (8 mol% yttria-stabilized zirconia, 8YSZ) and the Sr-containing lanthanum manganite (LSM) cathode are assembled between steel intercell connecting bipolar plates to stack several such cells together. Several problems arising due to the atomic diffusion across the interfaces at the high temperatures of SOFC oper-

ation has led to research on alternate materials and components for their operation at an intermediate temperature range (700–800°C) without the drawback of performance loss. New oxide-ion-conducting solid electrolytes [9–12], ceramic cathodes [13–15], nickel–cermet anodes [16–18] and interconnecting materials [19,20] were investigated for this purpose. In this research work, an experimental characterization of the ceramic high T_c superconducting phases $Bi_2Sr_2CaCu_2O_{8+x}$ (BSCC-2212) and $Bi_2Sr_2CuO_{6+x}$ (BSCC-2201) was carried out to see whether they can be useful as contact layer material between the LSM cathode and ferritic steel interconnects in planar IT-SOFCs. Preparation and characterization of the materials was closely adapted to SOFC requirements, that is, the synthesis of the powders was carried out only in air and not in pure oxygen and no sophisticated methods for textured microstructures were applied. The experimental results obtained from this research work are presented and a brief discussion of their thermal and electrical characteristics at SOFC operating temperatures is given referring to the special boundary conditions for this application. In a second publication we will report on chemical interaction with ferritic steels and cathode material during

† To whom all correspondence should be addressed. Tel.: +49-2461-615007; fax: +49-2461-2455.
E-mail address: f.tietz@fz-juelich.de (F. Tietz)

exposure at high temperatures [21].

2. EXPERIMENTAL

2.1. Synthesis of ceramic powders

Superconductor powders were prepared by the solid-state reaction technique, that is, by mixing and firing the corresponding oxides, nitrates or carbonates, and by the citrate complexation technique. Depending on the preparation route, the powders obtained are termed MO and CC, respectively.

In the solid-state reaction technique, appropriate molecular quantities of the starting precursors (Bi_2O_3, 99.99%; $Ca(NO_3)_2 \cdot 4H_2O$, 99.9%; CuO, 99.99% and $SrCO_3$, 99.99%, Bi_2O_3 from Aldrich, all other chemicals from Merck) were weighed and mixed well. The resulting mixtures were ball-milled with acetone and zirconia balls for 24 h under standardized conditions. After drying at 100°C for 2 h, they were once again ground well to achieve homogenization and subjected to sintering at 800°C for 24 h in air using clean alumina crucibles. After this process, the sintered oxides were crushed and powdered manually in an agate mortar. The powders obtained after the sintering procedure were black in color.

In the citrate complexation (CC) technique [22], the exact weights of the above mentioned precursor materials were taken and dissolved in distilled water with a very small quantity of nitric acid wherever necessary. The resulting solutions were mixed with citric acid solution already prepared in the molar ratio of 4 mol of citric acid to 1 mol of the metal cations and stirred well. These blue-colored solutions were continuously stirred while being heated at 80°C. After 3 h exactly 1 ml of ethylene glycol to 1 g of citric acid was added to the warm solutions in steps of 20 ml. The volume of ethylene glycol added to the solutions was a little more than the stoichiometric composition necessary to effect complete polyesterification with the citric acid present in the

solutions. These mixtures were heated at 220°C and stirred continuously until most of the solvent had evaporated. The viscosity of the hot solutions was observed to decrease with time and stirring became extremely difficult. The color of the solutions turned to deep brown and then to black. During this preparation, ignition was observed with the evolution of a deep brown stream of nitrogen oxides. The black masses obtained after complete evaporation were like resins and were dried in an oven in air at 230°C for several hours until they became coarse powders. These powders were subjected to calcination in two steps. In the first precalcination step, the coarse black materials were heated in air at 600°C for 3 h in a clean platinum crucible. This was carried out in a small furnace equipped with a gas-removing device in order to avoid the harmful effects of nitrogen oxides and the burn-out of organic residues. The powders obtained after precalcination were deep green in color. In the second calcination step, these green powders were annealed in air at 800°C for 24 h in an alumina crucible. No annealing in oxygen was carried out, because SOFCs operate with air as cathode gas. After calcination the samples were black in color and they were ground well prior to further measurements.

For the investigations with $YBa_2Cu_3O_{7-x}$ (YBCO) a commercial powder was used supplied by Solvay Barium and Strontium GmbH, Germany.

2.2. Preparation of compact pellets and sintering

For preparing circular (8 mm diameter) and rectangular pellets (40 mm length, 4 mm width, 5 mm thickness) from the powders, one to two drops of 2% solution of polyvinyl alcohol in distilled water were added as a binder to 1 g and about 3 g of powder, respectively. A homogeneous mixture of the powder and binder was made and subjected to uniaxial compression for 1 min at pressures of 300 MPa for circular pellets and 400 MPa for rectangular pellets. The circular pellets were subjected to various sintering

Table 1. Elemental analysis data obtained on the powder samples

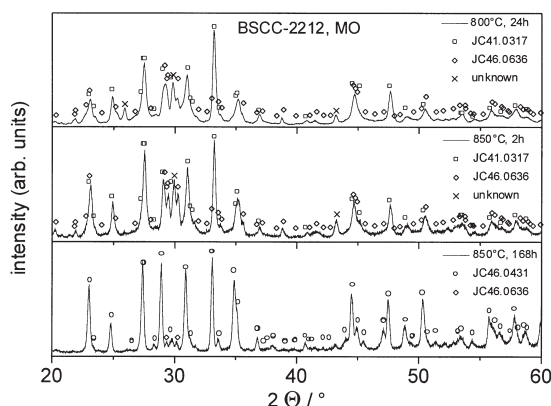| Sample	Element	Weight percentages		Analytical composition
		Calculated	Experimental	
$Bi_2Sr_2CaCu_2O_{8+x}$ (solid-state technique)	Bi	47.01	44.7	$Bi_{1.97}Sr_{2.04}Ca_{1.02}Cu_{1.97}O_{8+x}$
	Sr	19.69	18.7	
	Ca	4.525	4.42	
	Cu	14.31	13.1	
$Bi_2Sr_2CaCu_2O_{8+x}$ (citrate technique)	Bi	47.01	42.5	$Bi_{2.01}Sr_{2.01}Ca_{1.04}Cu_{1.94}O_{8+x}$
	Sr	19.69	18.5	
	Ca	4.525	4.22	
	Cu	14.31	12.9	
$Bi_2Sr_2CuO_{6+x}$ (solid-state technique)	Bi	53.22	53.0	$Bi_{2.01}Sr_{2.01}Cu_{0.98}O_{6+x}$
	Sr	22.29	22.2	
	Ca	–	–	
	Cu	8.12	7.84	
$Bi_2Sr_2CuO_{6+x}$ (citrate technique)	Bi	53.22	54.9	$Bi_{2.12}Sr_{1.98}Cu_{0.89}O_{6+x}$
	Sr	22.29	21.5	
	Ca	–	–	
	Cu	8.12	7.02	

Fig. 1. XRD patterns of the BSCC-2212 powder made via the mixed oxide route showing the evolution of phases. Top, after sintering at 800°C for 24 h; middle, after subsequent sintering at 850°C for 2 h; bottom, after subsequent sintering at 850°C for 168 h. The symbols refer to the JCPDS powder diffraction files 41-0317 ($Bi_2Sr_2CaCu_2O_{8+x}$), 46-0636 ($CuSr_2Bi_2O_6$) and 46-0431 ($Bi_{2.1}Sr_{1.9}CaCu_2O_{8.21}$) [23].

Fig. 3. XRD patterns of the BSCC-2201 powder made via the mixed oxide route showing the evolution of phases. Top, after sintering at 800°C for 24 h; middle, after subsequent sintering at 850°C for 2 h; bottom, after subsequent sintering at 850°C for 168 h. The symbols refer to the JCPDS powder diffraction files 39-0283 ($Bi_2Sr_2CuO_x$), 46-0636 ($CuSr_2Bi_2O_6$) and 43-0028 ($Sr_8Bi_4Cu_5O_x$) [23].
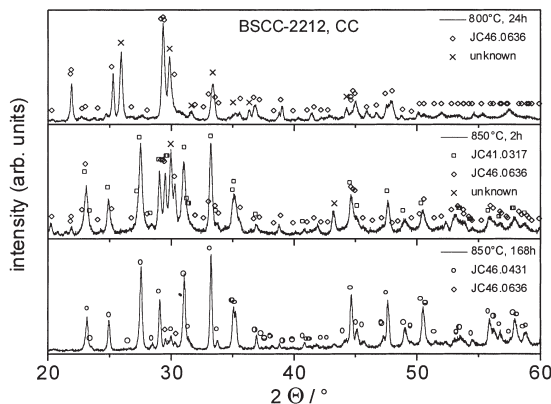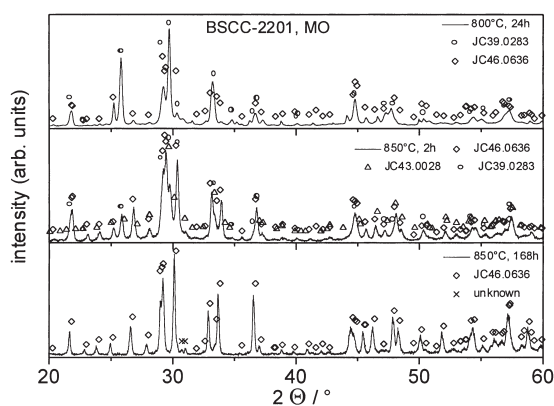

Fig. 2. XRD patterns of the BSCC-2212 powder made via the citrate complexation route showing the evolution of phases. Top, after sintering at 800°C for 24 h; middle, after subsequent sintering at 850°C for 2 h; bottom, after subsequent sintering at 850°C for 168 h. The symbols refer to the JCPDS powder diffraction files 41-0317 ($Bi_2Sr_2CaCu_2O_{8+x}$), 46-0636 ($CuSr_2Bi_2O_6$) and 46-0431 ($Bi_{2.1}Sr_{1.9}CaCu_2O_{8.21}$) [23].
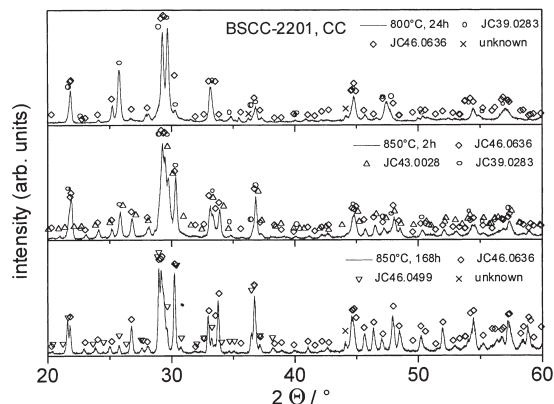

Fig. 4. XRD patterns of the BSCC-2201 powder made via the citrate complexation route showing the evolution of phases. Top, after sintering at 800°C for 24 h; middle, after subsequent sintering at 850°C for 2 h; bottom, after subsequent sintering at 850°C for 168 h. The symbols refer to the JCPDS powder diffraction files 39-0283 ($Bi_2Sr_2CuO_x$), 46-0636 ($CuSr_2Bi_2O_6$), 43-0028 ($Sr_8Bi_4Cu_5O_x$) and 46-0499 ($Sr_{1.8}CuBi_{2.2}O_{6.1}$) [23].

conditions with a view to investigating their volume shrinkage and to determining the densification behavior as a function of the sintering temperature in air. The sintering procedure involved a heating rate of 120K/h up to the final temperature, 2 h dwell time and a 180K/h cooling rate down to the room temperature. The final temperature of sintering was set at different levels between 700 and 850°C at 25°C intervals. Each sintering experiment was carried out on two identically prepared pellets.

The rectangular sticks were subjected to sintering at 800°C for 24 h initially and then at 850°C for 2 h. Since the information obtained from the X-ray diffraction (XRD) data indicated that the phase formation was not yet complete, these pellets were further subjected to sintering at 850°C for 1 week (168 h) to ensure complete formation of the superconducting phase.

2.3. Specimen characterization

The powders obtained after calcination were analytically investigated by inductively coupled plasma-atomic emission spectrometry (ICP-AES) performed on aqueous solutions obtained by dissolving the powders in nitric acid to find the elemental composition of Ba, Sr, Ca, and Cu. The results obtained are presented in Table 1. The observed deviations from the nominal compositions were within the precision of the instrument (±3 wt%).

Scanning electron microscopy (SEM) of the powder particles and the microstructure of the cross sections of the annealed pellets was carried out with the scanning electron microscope Jeol JSM T300. The

powder samples were subjected to XRD analysis using a Siemens D5000 apparatus with CuK$_\alpha$ radiation to ascertain the formation of the desired crystallographic phases and to examine whether there were any additional phases. Differential thermal analyses (DTA) combined with thermogravimetry (TG) were carried out in a Netzsch STA 409 to detect the melting points and the crystallization behavior of the different powders. The particle size distribution of the powders was obtained in a computer-controlled laser diffraction particle size analyzer (Malvern, Easy Particle Sizer Model 3.0) using sodium pyrophosphate

buffer after dispersing the powders in methanol. The density values were calculated from weight/volume ratios and by the Archimedes method. The surface area of the powders was determined by the Brunauer–Emmett–Teller (BET) method using a surface area analyzer (Quantasorb, QS-14).

The electrical conductivity of the pellets was measured by a standard four-point DC technique. Pt paste and wire were used to ensure good contacts on the pellets. The measurements were carried out in air up to 900°C at defined temperature intervals. The thermal expansion measurements were carried out with a Netsch DIL 402 E dilatometer.

3. RESULTS AND DISCUSSION

3.1. Powder characteristics

The color of the powders was black for all the four samples investigated. The elemental analysis results of the cations shown in Table 1, obtained on the powders after calcination at 800°C for 24 h, indicate a good agreement between nominal and analytical composition. Only the Bi and Cu contents of the BSCC-2201 powder made by the CC technique show a deviation from the nominal composition of >5%. The morphology of the powder particles was similar for all powders and consisted of agglomerates of up to 50 μm. The larger grains, that is, in the 10–50 μm range, already had an anisotropic appearance but micrometer-sized grains were usually globular.

The XRD results obtained are presented in Figs 1–4 and indicate that the phase evolution was completed only after long-term continuous calcination of the powder. Evidence for the existence of other phases was observed in all batches during short annealing times and was stronger for the powders obtained by citrate complexation. In the case of BSCC-2212 powders large amounts of BSCC-2201 were found which disappeared during long annealing times (Figs 1 and 2). Both BSCC-2201 powders (Figs 3 and 4) contained two slightly different crystal structure modifications of this compound after sintering at 800°C, but no additional phases. However, after brief annealing at 850°C small amounts of $Sr_8Bi_4Cu_5O_x$ were formed which disappeared again after long heat treatments. In the case of the BSCC-2201 powder prepared by the CC technique, some additional reflections of the XRD pattern of $Bi_{2.2}Sr_{1.8}CuO_{6.1}$ [23] were observed (Fig. 4, bottom), which reflect the compositional devi-
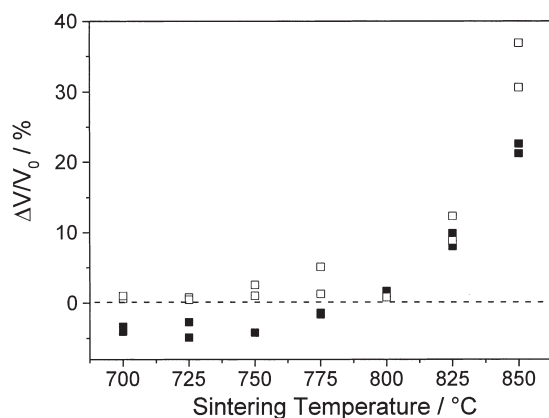

Fig. 5. Relative volume change of BSCC-2212 pellets versus annealing temperature after 2 h dwell time at the given temperatures (■, MO powder; □, CC powder).
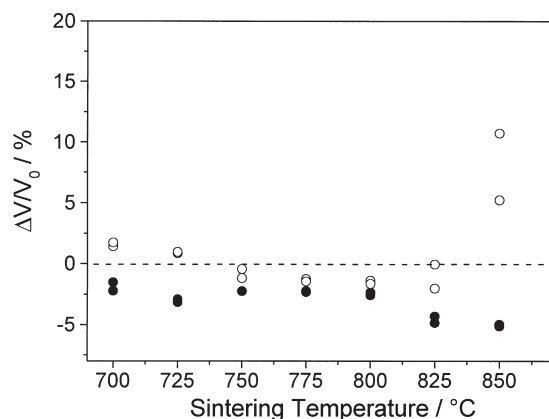

Fig. 6. Relative volume change of BSCC-2201 pellets versus annealing temperature after 2 h dwell time at the given temperatures (■, MO powder; □, CC powder).

Table 2. Physical characteristics obtained on the powder samples

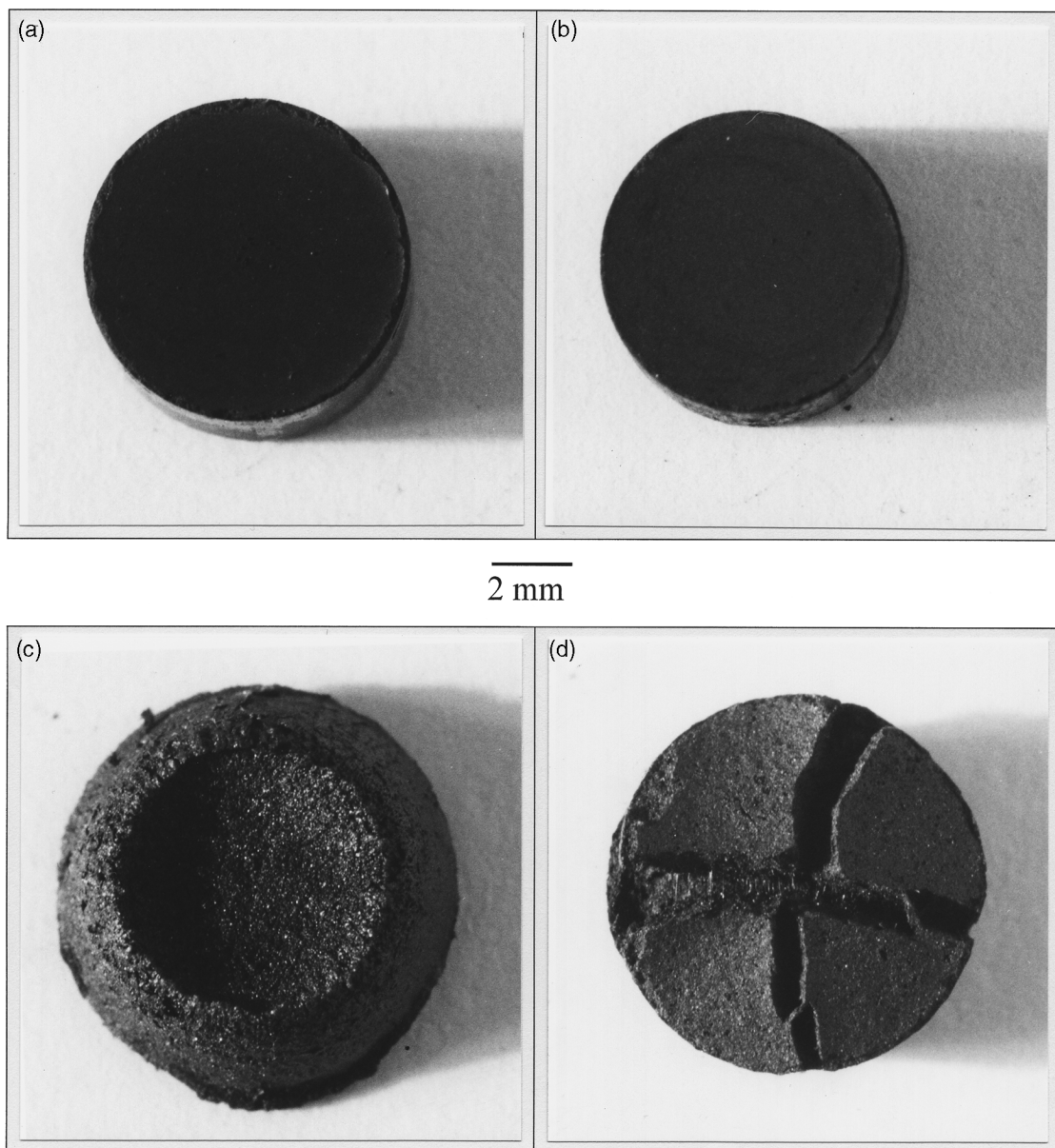| Sample	d_{50} (μm)	Apparent powder density (g cm^{-3})	Tap density (g cm^{-3})	BET surface area (m^2 g^{-1})
$Bi_2Sr_2CaCu_2O_{8+x}$ (solid-state technique)	7.4	2.22	3.36	8.31
$Bi_2Sr_2CuO_{6+x}$ (solid-state technique)	6.5	2.46	3.61	7.62
$Bi_2Sr_2CaCu_2O_{8+x}$ (citrate technique)	3.6	2.96	3.57	9.54
$Bi_2Sr_2CuO_{6+x}$ (citrate technique)	4.5	2.76	3.35	12.83
$YBa_2Cu_3O_{7-x}$ (commercial)	5.5	1.25	2.16	6.17

Fig. 7. Photographs of the BSCC-2201 pellets (solid-state reaction) showing the evolution of expansion and cracks as a function of annealing temperature: (a) as prepared, (b) annealed at 825°C/2 h, (c) annealed at 850°C/2 h, (d) annealed at 860°C/2 h.

ation from the nominal composition as found by chemical analysis (Table 1). The powder morphology varied little. The particle size data (d_{50} values), the apparent powder and tap density data and the BET surface area values obtained on the powders are presented in Table 2. The apparent powder density and the tap density of the powders did not vary significantly although different methods were adopted for their synthesis. The particle size distribution function obtained from these powders was uniform. The

particle sizes of these powders, that is, 5–10 μm, were small enough to fabricate the pellets for further measurements.

The DTA experiments indicated melting points of 838 and 896°C for BSCC-2212 and BSCC-2201, respectively, both produced by the solid-state reaction technique and 836°C for the BSCC-2212 made by the citrate complexation technique. The DTA curves showed only broad endothermic peaks up to 800°C, which was related to the onset of oxygen loss
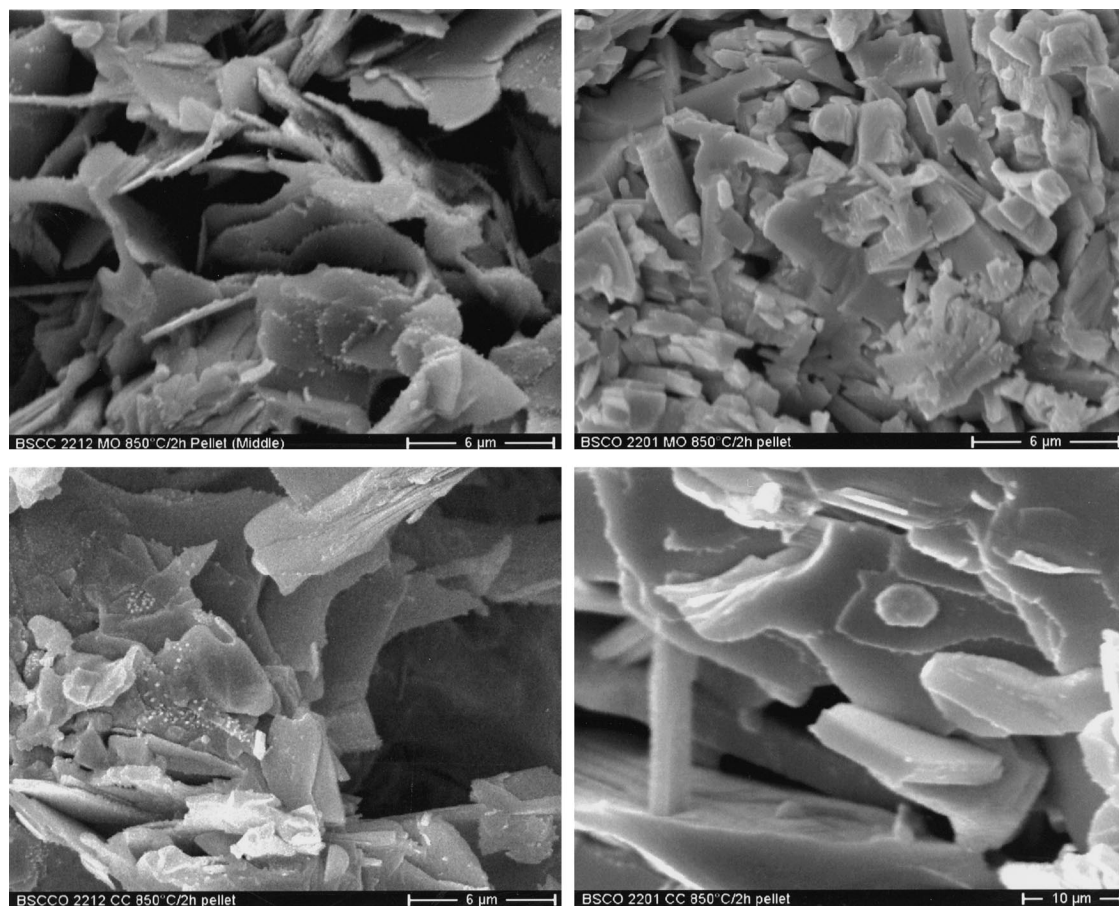
Fig. 8. SEM pictures showing the particle morphology of the ceramic powders after pressing to pellets and sintering at 850°C for 2 h. Top row, MO powders; bottom row, CC powders. Left, BSCC2212 powders; right, BSCC2201 powders. Note that the magnification for BSCC2201 (CC) is different from the other samples.

observed in the TG curves. Reversible oxygen loss and gain was observed during the heating and cooling cycle.

3.2. Densification and microstructure

The green pellets fabricated from the powders under identical conditions were subjected to different sintering conditions to understand their thermal characteristics. The results obtained from the annealing experiments were used to estimate the relative volume changes as a function of the annealing temperature and are presented in Figs 5 and 6 for BSCC-2212 and BSCC-2201, respectively.

The photographs of the pellets taken before and after annealing under different temperature conditions are shown in Fig. 7. From the expansion curves obtained on BSCC-2212 pellets, it was inferred that the relative expansion due to annealing was almost linear up to a temperature of 800°C and above this point it increased abruptly up to 850°C. BSCC-2201 showed less relative expansion as a function of annealing temperature than BSCC-2212. Another observation made from these curves and the photo-

graphs was that there was competition between the densification of the pellets and phase evolution involving crystallization and anisotropic grain growth resulting in volume expansion and cracks. The results of these furnace sintering experiments are readily comparable with sintering curves recorded during constant heating in a dilatometer [24]. There was a wide difference observed in the relative expansion behavior of the BSCC-2201 pellets fabricated from the two powders.

The microstructures of the powders after 2 h annealing at 850°C are presented in Fig. 8. No globular particles are observed in any of them. BSCC-2212 (MO) (top left in Fig. 8) consists of thin platelets, also as does BSCC-2212 (CC) but mixed together with irregularly shaped grains (bottom left in Fig. 8). BSCC-2201 (MO) is the only exception with elongated rod-like grains. The platelets observed in this case are much thicker and more densely packed than in the others cases. BSCC-2201 (CC) also shows thin platelets, but the XRD pattern is very similar to that of the BSCC-2201 (MO) powder (Figs 3 and 4). A longer annealing time of 168 h did not significantly
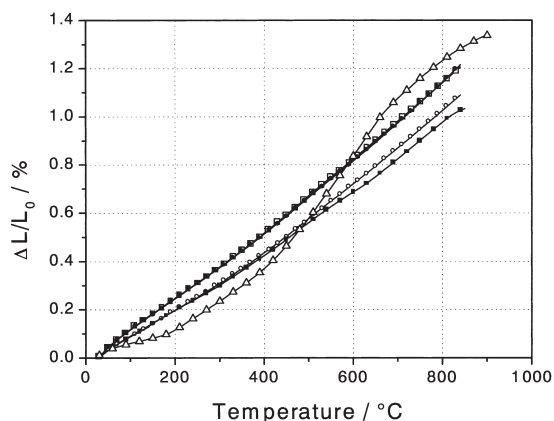
Fig. 9. Thermal expansion curves of the ceramics BSCC-2201 [CC powder after annealing at 850°C for 24 h (□), CC powder after annealing at 850°C for 168 h (○), MO powder after annealing at 850°C for 168 h (●)], BSCC-2212 [CC powder after annealing at 850°C for 24 h (■)] and YBCO [after annealing at 850°C for 168 h (△)].
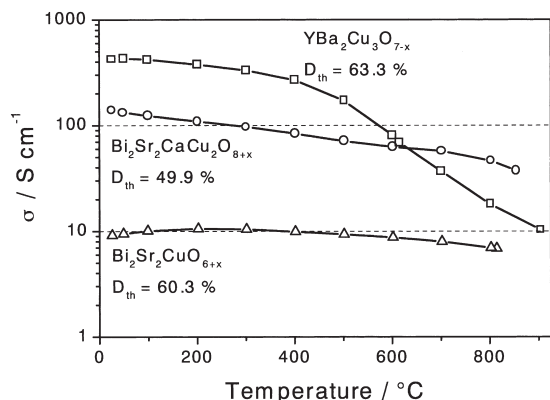

Fig. 10. Electrical conductivity versus temperature for YBCO, BSCC-2212 (MO), and BSCC-2201 (MO) after long-term annealing at 850°C in air.

change the morphology of the grains. However, the "pores", that is, the distances between adjacent grains, seemed to be larger than shown in Fig. 8.

From the XRD patterns it is evident that enrichment of the desired phase is a progressive trend as a function of annealing temperature and time (Figs 1–4, bottom). The grain growth taking place during phase re-arrangement of the powders clearly indicated that the volume expansion observed on the pellets is due to the preferred growth in the crystallographic *a–b* plane combined with a mutual displacement with increasing distance.

3.3. Thermal expansion

The thermal expansion curves significantly depended on the preparation route and phases present in the specimen. To avoid influences from sintering or crystallization processes during heating, the cooling curves for the bismuth cuprate samples were used. Such differences can be seen well in Fig. 9 for the

various BSCC-2201 samples measured. After sintering at 850°C for 24 h, the BSCC-2201 sample made from the CC powder showed a larger thermal expansion than after annealing for 168 h. The thermal expansion coefficient (TEC) between 30 and 800°C decreased from 14.5 to $13.3 \times 10^{-6} K^{-1}$. Neither sample was single-phase but contained different additional phases transformed during heat treatment (see Fig. 4). The other BSCC-2201 sample made from the MO powder was single-phase after 168 h. Therefore this curve can be regarded as the expansion curve for pure $Bi_2Sr_2CuO_{6+x}$ with a TEC of $14.8 \times 10^{-6} K^{-1}$. By chance, it coincides with the curve of BSCC-2201 made by CC and heat-treated for 24 h at 850°C.

The BSCC-2212 sample exhibited the smallest expansion of all investigated cuprates (Fig. 9) with a TEC of $12.7 \times 10^{-6} K^{-1}$. This value is in very good agreement with the thermal expansion of the currently used interconnect, anode and cathode materials [25]. Single-phase BSCC-2212 samples obtained after long-term annealing at 850°C were too brittle for measurement and broke during handling.

Finally, the S-shaped expansion curve of YBCO is also shown in Fig. 9 yielding a TEC of $16.0 \times 10^{-6} K^{-1}$ between 30 and 800°C. The steep increase in the expansion curve of $YBa_2Cu_3O_{7-x}$ was attributed to the orthorhombic–tetragonal phase transition [26] and the expansion of the polycrystalline sample mainly reflects the temperature-dependent changes of the *c*-lattice parameter. The measurement on YBCO is in good agreement with data given in Ref. [27]. Another investigation dealing with high-temperature dilatometry on superconductor materials, however, led to much higher thermal expansions for YBCO [28] and lower values for BSCC-2212, which might be due to sintering or pressure-induced length changes.

3.4. Electrical conductivity

Electrical conductivity values measured on the rectangular pellets fabricated from the ceramic powders are presented in Fig. 10 as a function of temperature. The data points were recorded during cooling with isothermal sections for measurements. It should be emphasized that no efforts were made to strongly densify the samples to obtain relative density values (D_{th}) which can be expected after SOFC assembly conditions. Therefore only relative densities between 50 and 65% were achieved (Fig. 10). At a temperature of 800°C, conductivity values of 18, 46 and 7 S cm^{-1} were recorded for YBCO, BSCC-2212 and BSCC-2201, respectively. All the samples showed metallic behavior at high temperatures, in particular YBCO showed a steep conductivity decrease after the orthorhombic–tetragonal phase transition [27, 30] due to loss of oxygen [26]. Due to the low density of the specimens investigated here, the conductivities may be lower than previously reported [27, 30], but in the case of YBCO, the measured values are in excellent agreement with previous data [29]. The values at

800°C are at the lower limit for their SOFC application as a contact layer [6, 31]. As a rule of thumb the conductivity of such contact materials should not be lower than 10 S cm^{-1} at operating temperature.

4. CONCLUSION

It has been shown that the superconducting ceramic materials $Bi_2Sr_2CaCu_2O_{8+x}$, $Bi_2Sr_2CuO_{6+x}$ and $YBa_2Cu_3O_{7-x}$ offer acceptable electrical and thermal properties for application as thin contact layer material at the interface between the LSM cathode and ferritic steel interconnector in IT-SOFCs. However, the sintering experiments showed not only inadequate sintering activity even at temperatures close to the melting points but also an abrupt increase in volume due to crystallization and anisotropic grain growth. For SOFC applications, it is necessary to decouple the sintering from the phase evolution observed on both $Bi_2Sr_2CaCu_2O_{8+x}$ and $Bi_2Sr_2CuO_{6+x}$ ceramics at temperatures above 800°C.

REFERENCES

1. Glaser, S. and Escombe, F., in: Ph. Stevenson ed., *Proc. 3rd Eur. SOFC Forum*, Nantes, 1998, vol. 1, p. 45.
2. Kim, J., Virkar, A. V., Fung, K., Mehta, K. and Singhal, S. C., *J. Electrochem. Soc.*, 1999, **146**, 69.
3. Williams, M. C., in *Proc. 6th Int. Symp. Solid Oxide Fuel Cells (SOFC-VI)*, Vol. 99-19, ed. S. C. Singhal and M. Dokiya. The Electrochemical Society, Pennington, NJ, 1999, p. 3.
4. Godfrey, B., Gillespie, R. and Föger, R., in *Proc. 6th Int. Symp. Solid Oxide Fuel Cells (SOFC-VI)*, Vol. 99-19, ed. S. C. Singhal and M. Dokiya. The Electrochemical Society, Pennington, NJ, 1999, p. 75.
5. Krist, K., Gleason, K. J. and Wright, J. D., in *Proc. 6th Int. Symp. Solid Oxide Fuel Cells (SOFC-VI)*, Vol. 99-19, ed. S. C. Singhal and M. Dokiya. The Electrochemical Society, Pennington, NJ, 1999, p. 107.
6. Minh, N. Q., *J. Am. Ceram. Soc.*, 1993, **76**, 563.
7. Murugesamoorthi, K. A., Srinivasan, S. and Appleby, A. J., in *Fuel cell systems*, ed. L. J. M. J. Blomen and M. N. Mugerua. Plenum Press, New York, 1993, p. 464.
8. Arul Raj, I. and Venkatesan, V. K., *Int. J. Hydrogen Energy*, 1988, **13**, 215.
9. Feng, M. and Goodenough, J. B., *Eur. J. Solid State Inorg. Chem.*, 1994, **31**, 663.
10. Huang, P. and Petric, A., *J. Electrochem. Soc.*, 1996, **143**, 1644.
11. Yamamoto, O., Arati, Y., Takeda, Y., Imanishi, N., Mizutani, Y., Kawai, M. and Nakamura, Y., *Solid State Ionics*, 1995, **79**, 137.
12. Tietz, F., Fischer, W., Hauber, Th. and Mariotto, G., *Solid State Ionics*, 1997, **100**, 289.
13. Tsai, T. and Barnett, A., in *Proc. 5th Int. Symp. Solid Oxide Fuel Cells (SOFC-V)*, Vol. 97-40, ed. U. Stimming, S. C. Singhal, H. Tagawa and W. Lehnert. The Electrochemical Society, Pennington, NJ, 1997, p. 369.
14. Tai, L. -W., Nasrallah, M. M., Anderson, H. U., Sparlin, D. M. and Sehlin, S. R., *Solid State Ionics*, 1995, **76**, 259 and 273.
15. Ullmann, H., Trofimenko, N., Tietz, F., Stöver, D. and Ahmad-Khanlou, A., *Solid State Ionics*, 2000, **138**, 79.
16. Maric, R., Ohara, S., Fukui, T., Inagaki, T. and Fujita, J., *Electrochem. Solid State Lett.*, 1998, **1**, 201.
17. Costamagna, P., Costa, P. and Arato, E., *Electrochim. Acta*, 1998, **43**, 967.
18. Mori, M., Yamamoto, T., Itoh, H., Inaba, H. and Tagawa, H., *J. Electrochem. Soc.*, 1998, **145**, 1374.
19. Quadakkers, W. J., Greiner, H., Hänsel, M., Pattanaik, A., Khanna, A. S. and Malléner, W., *Solid State Ionics*, 1996, **91**, 55.
20. Schmidt, H., Bruckner, B. and Fischer, K., in *Proc. 4th Int. Symp. Solid Oxide Fuel Cells (SOFC-IV)*, ed. M. Dokyia, O. Yamamoto, H. Tagawa and S. C. Singhal, The Electrochemical Society, Pennington, NJ, 1995, p. 869.
21. Tietz, F., Arul Raj, I., Gupta, A., Wessel, E., and Stöver, D., Part II of this series of publications (in preparation).
22. Pechini, M. P., US Patent No. 3,330,697, July 1967.
23. Updated JCPDS database of the International Centre for Diffraction Data, Newton Square, Pennsylvania (1998).
24. Tietz, F., Gupta, A., Jungen, W., Wessel, E., Arul Raj, I. and Stöver, D., in: *Proc. 1st Int. Conf. Adv. Mater. Processing*, Rotorua (New Zealand), November 2000. ed. D. L. Zhang, K. L. Pickering and X. Y. Xiong, Institute of Materials Engineering Australia Ltd., 2000, p. 385.
25. Tietz, F., *Ionics*, 1999, **5**, 129.
26. Jorgensen, J. D., Beno, M. A., Hinks, D. G., Soderholm, L., Volin, K. J., Segre, C. U., Zhang, K. and Kleefisch, M. S., *Phys. Rev. B*, 1987, **36**, 3608.
27. Petrov, G. S., Clyndyuck, A. I., Maasyuck, S. V., Bashkirov, L. A. and Akimov, A. I., *High Temp.–High Press.*, 1998, **30**, 483.
28. Momin, A. C., Mirza, E. B. and Mathews, M. D., *Int. J. Thermophys.*, 1991, **12**, 585.
29. Patil, D. S., Karthikeyan, J., Venkatramani, N. and Rohatgi, V. K., *J. Mater. Sci. Lett.*, 1989, **8**, 1199.
30. Munakata, F., Shinohara, K. and Yamanaka, M., *Jap. J. Appl. Phys.*, 1989, **28**, L34.
31. Minh, N. Q. and Takahasi, T., in *Science and Technology of Ceramic Fuel Cells*, Elsevier Science, The Netherlands, 1995, p. 129.